Improved Sliding Mode Traction Control Combined Sliding Mode Disturbance Observer Strategy for High-Speed Maglev Train

Xueqian Cao, Qiongxuan Ge, *Member, IEEE*, Jinquan Zhu, Ganlin Kong, Bo Zhang, and Xiaoxin Wang

***Abstract*—To improve the robustness and dynamic tracking performance of the stator current control for the long stator linear synchronous motor (LSLSM) used in high-speed maglev train traction system, a composite current control strategy combining a sliding mode current controller (SMCC) and a sliding mode disturbance observer (SMDO) is proposed in this article. First, the LSLSM mathematical model in double feed mode is optimized. Then, an SMCC is designed based on the model. An improved stability criterion is proposed and the SMCC switching gain is obtained quantitatively to meet the current following speed required for the stator changeover process. As disturbance factors, parameter perturbation of the LSLSM and the stator changeover will bring about transient current fluctuations and chattering. Therefore, an SMDO is designed to estimate the disturbances and perform feed-forward compensation for the SMCC, thereby improving the robustness and suppressing the current chattering. Finally, the hardware-in-the-loop experiments verify the effectiveness of this strategy and compare it with the traditional current control strategy.**

***Index Terms*—High-speed maglev, long stator linear synchronous motor (LSLSM), sliding mode current control (SMCC), sliding mode disturbance observer (SMDO), stator changeover.**

I. Introduction

MAGLEV train avoids the loss caused by wheel-rail contact and adhesion, thereby improving efficiency and being more suitable for long-distance transportation [1], [2]. The electromagnetic suspension (EMS) type high-speed maglev train is driven by two long stator linear synchronous motors (LSLSMs) on the left and right sides, and one side of the train with excitation magnetic pole and the track with armature windings can be regarded as the mover and stator, respectively.

Manuscript received 23 June 2022; accepted 19 August 2022. Date of publication 25 August 2022; date of current version 10 October 2022. This work was supported in part by National Natural Science Foundation of China under Grant 51907188, in part by the Institute of Electrical Engineering, CAS E155320201, and in part by Youth Innovation Promotion Association CAS 2021137. Recommended for publication by Associate Editor G. Konstantinou. *(Corresponding author: Qiongxuan Ge.)*

The authors are with the Key Laboratory of Power Electronics and Electric Drive, Institute of Electrical Engineering, Chinese Academy of Sciences, Beijing 100190, China, and also with the University of Chinese Academy of Sciences, Beijing 100049, China (e-mail: caoxueqian@mail.iee.ac.cn; gqx@mail.iee.ac.cn; zhujinquan@mail.iee.ac.cn; konggl@mail.iee.ac.cn; zhangbo@mail.iee.ac.cn; wxxhit@mail.iee.ac.cn).

Color versions of one or more figures in this article are available at https://doi.org/10.1109/TPEL.2022.3201614.

Digital Object Identifier 10.1109/TPEL.2022.3201614

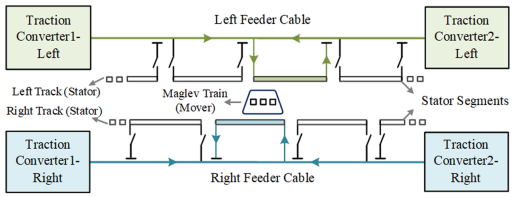

Fig. 1. Traction system structure with step-by-step segmented method in DF mode.

As two important parts of high-speed maglev train, traction and suspension systems share a set of excitation poles [3], [4]. The traction system studied in this article has the following special features: a) the long stator adopts a step-by-step segmented method, which does not require additional converters, and the process of staggered switching between the left and right stator segments is called stator changeover, and b) under low-speed operation, a traction converter with a capacity of 24 MVA at one end of the line feeds the stator segment where the train is located through the feeder cable, which operates in single feed (SF) mode; under high-speed operation, the traction converters at both ends feed the stator segment at the same time, which operates in double feed (DF) mode [5], [6]. Fig. 1 shows the traction system structure with step-by-step segmented method in DF mode.

To decouple the traction system and suspension system, the LSLSM adopts the field oriented control (FOC) method with $i_d = 0$ [5]. For the traction system, the traction force of the train is indirectly controlled by adjusting the stator current to achieve smooth and precise operation [7], [8]. Therefore, the stator current control is the key technology of the traction system. At present, the traction system mainly adopts a traditional stator current control strategy of proportional integral combined with voltage feed-forward decoupling (PI-VFDC). However, the attenuation and recovery rate of the reference current can reach thousands of amperes per second during the changeover process. Due to the lack of robustness and dynamic following performance of the traditional control strategy, the sharp current change will make it difficult for the actual current to follow the reference current in time and produce large transient fluctuations, which can lead to the failed completion of the stator switching action. In addition, the parameters of the motor and feeder cable are prone to perturbation in a

complex working environment, which leads to uncertainty in stator current control and affects the stability and accuracy of train operation. Therefore, a high-performance stator current control strategy suitable for the special working conditions of high-speed maglev train needs urgent study.

At present, many methods have been proposed for the stator current control, such as predictive control [9], [10], [11], [12], robust control [13], [14], internal model control (IMC) [15], [16], adaptive control [17], and sliding mode control (SMC) [18], [19], [20], [21], [22], [23]. Among them, SMC has attracted wide attention due to its insensitivity to disturbances, fast response, and easy realization. SMC usually adopts a sign function with high switching gain to ensure its robustness and response speed [24]. However, since the upper bound of the disturbance is unpredictable, a higher switching gain must be selected to provide stronger robustness, which can introduce strong current chattering. Various methods have been proposed to suppress chattering, such as improving sign function [20], sliding surface [21], [22], and reaching law [23]. However, high-power or large-inertia systems, such as high-speed maglev trains, are not sensitive enough to these improvements and the dynamic tracking performance may be compromised.

Designing an observer to estimate the disturbances and compensate for SMC is an attractive proposition that allows the switching gain to be reduced only to meet the required current following speed without loss of robustness. Researchers have proposed disturbance observer (DOB) [25], [26], extended state observer (ESO) [27], [28], [29], and sliding mode disturbance observer (SMDO) [30], [31], [32], [33], [34], [35], [36]. Among them, SMDO also has the advantages of simple implementation, fast response, and strong robustness. In [30], [31], [32], and [33], an SMDO was combined with predictive control to improve the robustness of current control. In [34] and [35], a composite sliding mode control strategy consisting of an SMC based on a new reaching law and an extended sliding mode disturbance observer (ESMDO) was proposed, which realized the high-precision control of the motor speed loop. In [36], the disturbance and mechanical parameters of the motor were observed, and a low-pass filter was designed to suppress chattering. These studies show that the SMDO can compensate the disturbance effectively.

In this article, a composite stator control strategy for the LSLSM used in high-speed maglev train in DF mode based on SMCC and SMDO is proposed. The SMCC is designed according to the optimized LSLSM mathematical model. To meet the required current following speed, the Lyapunov stability criterion is improved. The quantitative switching gain is obtained by narrowing the stability range of the criterion, which makes the current state variable reach the sliding surface in finite time. In addition, the sliding mode reaching law is also improved. Then, the disturbance estimated by the SMDO is used as feed-forward compensation for the SMCC to reduce chattering and enhance robustness.

The remainder of this article is organized as follows. Section II optimizes the LSLSM mathematical model in DF mode and introduces the disturbances. Section III designs the SMCC and focuses on the proposed method for obtaining appropriate switching gain. Then, the SMDO is designed in Section IV. In Section V, the hardware-in-the-loop (HIL) experimental results verify the effectiveness of the proposed strategy. Finally, Section VI concludes this article.

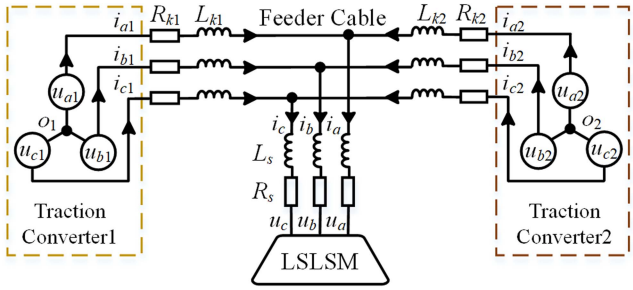

Fig. 2. Equivalent circuit of the LSLSM in DF mode.

II. Machine Mathematical Model

A. Mathematical Model of the LSLSM in DF Mode

DF mode is a particular power feed mode for high-speed maglev trains, as shown in Fig. 2. The essence of DF mode is that two sets of traction converters are connected in parallel and feed the stator segment where the train is running through the feeder cable. There is a nonnegligible voltage drop on the feeder cable. Therefore, unlike the conventional linear synchronous motors, in addition to the stator covered by the train, the feeder cable also needs to be considered when establishing the LSLSM mathematical model.

Based on [2], with the output currents of the inverters at both ends as the state variables and the output voltages of the inverters as the input variables, the *dq*-axis mathematical model of the LSLSM in DF mode is established as (1) shown at the bottom of the next page where

$$\omega = \pi v/\tau, \psi_m = M_{sm} i_m$$

u_{d1}, u_{q1}, i_{d1}, and i_{q1} are the *dq*-axis output voltages and output currents of the first converter; u_{d2}, u_{q2}, i_{d2}, and i_{q2} are the *dq*-axis output voltages and output currents of the second converter; L_d and L_q are the *dq*-axis stator inductances; R_s is the stator resistance; R_{k1}, R_{k2}, L_{k1}, and L_{k2} are the parameters of the feeder cables on both sides; ψ_m is the excitation flux linkage; M_{sm} is the mutual inductance between the stator and the excitation winding; i_m is the excitation current; v is the train speed; τ is the pole pitch ($\tau = 0.258$ m); ω is the angular velocity of the mover; and p is the differential operator.

According to Model (1), the stator current is indirectly controlled by controlling the output currents of the two converters. In addition, there is a circulating current between two converters, which increases the power loss of the system. To directly control the stator current and suppress the circulating current, the two converters can be regarded as an integral power feed system. The sum of the voltages output by the two converters and the difference between the voltages are taken as the input variables. The *dq*-axis stator currents jointly output by the two converters and the circulating currents are used as the state variables. The

optimized mathematical model of the LSLSM is derived as (2) shown at the bottom of this page, where unnumbered equation shown at the bottom of this page.

According to Model (2), the current control strategy can be designed as follows. The stator currents and the circulating currents are calculated from the output currents of the converters. The stator current controllers and the circulating current controllers are introduced to obtain the sum and difference of the output reference voltages of the two converters, so as to realize the direct control of the stator currents and circulating currents.

B. Model Considering Disturbances

The disturbances in Model (2) can be summarized as follows.

a) In a complex environment, the resistance and inductance parameters of the motor and feeder cables are prone to perturbation.

b) The circulating currents are suppressed to small values by the controllers. Therefore, the circulating currents in Model (2) can be regarded as small disturbances.

c) The transient current fluctuations caused by the stator changeover can be regarded as a kind of disturbance in Model (2).

Therefore, the LSLSM mathematical model considering the disturbances is as follows:

$$\begin{bmatrix} u_{dsum} \\ u_{qsum} \end{bmatrix} = \begin{bmatrix} R_{z0} + L_{dz0}p & -\omega L_{qz0} \\ \omega L_{dz0} & R_{z0} + L_{qz0}p \end{bmatrix} \begin{bmatrix} i_{dsum} \\ i_{qsum} \end{bmatrix} + \begin{bmatrix} 0 \\ 2\omega\psi_{sm0} \end{bmatrix} + \begin{bmatrix} f_d \\ f_q \end{bmatrix} \tag{3}$$

where

$$\begin{bmatrix} f_d \\ f_q \end{bmatrix} = \begin{bmatrix} \Delta R_z + \Delta L_{dz}p & -\omega\Delta L_{qz0} \\ -\omega\Delta L_{qz} & \Delta R_z + \Delta L_{qz}p \end{bmatrix} \begin{bmatrix} i_{dsum} \\ i_{qsum} \end{bmatrix} + \begin{bmatrix} 0 \\ 2\omega\Delta\psi_{sm0} \end{bmatrix} + \begin{bmatrix} \delta_d \\ \delta_q \end{bmatrix}$$

$$\begin{bmatrix} \Delta R_z \\ \Delta L_{dz} \\ \Delta L_{qz} \\ \Delta\psi_{sm} \\ \delta_d \\ \delta_q \end{bmatrix} = \begin{bmatrix} R_z - R_{z0} \\ L_{dz} - L_{dz0} \\ L_{qz} - L_{qz0} \\ \psi_{sm} - \psi_{sm0} \\ (L_{sub}p + R_{sub})i_{dsub} - \omega L_{sub}i_{qsub} + \xi_d \\ (L_{sub}p + R_{sub})i_{qsub} - \omega L_{sub}i_{qsub} + \xi_q \end{bmatrix}$$

f_d and f_q are the total disturbance terms in the *dq*-axis voltage equation; the subscript "0" represents the ideal value of the corresponding parameter; ΔR_z, ΔL_{dz}, ΔL_{qz}, and $\Delta\psi_{sm}$ are the perturbation values of the total resistance, the total inductance, and the mutual inductance parameters in *dq*-axis, respectively; ξ_d and ξ_q are the disturbance terms from current variations of the changeover and other uncertainties; δ_d and δ_q are the disturbance terms including ξ_d and ξ_q and the circulating current terms.

In Model (3), the disturbances are very complex. In addition, the disturbance caused by inductance perturbation is related to the train speed, so the influence of this disturbance is greater at high speed. Since the speed change of the train is relatively gentle and the value of the circulating current is small, the speed controller and the circulating current controllers can still use the PI controllers to meet the expected control effect. The stator current controllers must have strong robustness and high dynamic following performance.

$$\begin{bmatrix} u_{d1} \\ u_{q1} \\ u_{d2} \\ u_{q2} \end{bmatrix} = \begin{bmatrix} L_{k1}p + L_dp + R_{k1} + R_s & -\omega(L_{k1} + L_q) & L_dp + R_s & -\omega L_q \\ \omega(L_{k1} + L_d) & L_{k1}p + L_qp + R_{k1} + R_s & \omega L_d & L_qp + R_s \\ L_dp + R_s & -\omega L_q & L_2p + L_dp + R_{k2} + R_s & -\omega(L_{k2} + L_q) \\ \omega L_d & L_qp + R_s & \omega(L_{k2} + L_d) & L_{k2}p + L_qp + R_{k2} + R_s \end{bmatrix} \begin{bmatrix} i_{d1} \\ i_{q1} \\ i_{d2} \\ i_{q2} \end{bmatrix} + \begin{bmatrix} 0 \\ \omega\psi_m \\ 0 \\ \omega\psi_m \end{bmatrix} \tag{1}$$

$$\begin{bmatrix} u_{dsum} \\ u_{qsum} \\ u_{dsub} \\ u_{qsub} \end{bmatrix} = \begin{bmatrix} R_z + L_{dz}p & -\omega L_{qz} & L_{sub}p + R_{sub} & -\omega L_{sub} \\ \omega L_{dz} & R_z + L_{qz}p & \omega L_{sub} & L_{sub}p + R_{sub} \\ 0.5(R_{sub} + L_{sub}p) & -0.5\omega L_{sub} & L_{sum}p + R_{sum} & -\omega L_{sum} \\ 0.5\omega L_{sub} & 0.5(R_{sub} + L_{sub}p) & \omega L_{sum} & L_{sum}p + R_{sum} \end{bmatrix} \begin{bmatrix} i_{dsum} \\ i_{qsum} \\ i_{dsub} \\ i_{qsub} \end{bmatrix} + \begin{bmatrix} 0 \\ 2\omega\psi_m \\ 0 \\ 0 \end{bmatrix} \tag{2}$$

$$\begin{bmatrix} u_{dsum} \\ u_{qsum} \\ i_{dsum} \\ i_{qsum} \end{bmatrix} = \begin{bmatrix} u_{d1} + u_{d2} \\ u_{q1} + u_{q2} \\ i_{d1} + i_{d2} \\ i_{q1} + i_{q2} \end{bmatrix}, \begin{bmatrix} u_{dsub} \\ u_{qsub} \\ i_{dsub} \\ i_{qsub} \end{bmatrix} = \begin{bmatrix} u_{d1} - u_{d2} \\ u_{q1} - u_{q2} \\ 0.5(i_{d1} - i_{d2}) \\ 0.5(i_{q1} - i_{q2}) \end{bmatrix}, \begin{bmatrix} L_{sum} \\ L_{sub} \\ R_{sum} \\ R_{sub} \end{bmatrix} = \begin{bmatrix} L_{k1} + L_{k2} \\ L_{k1} - L_{k2} \\ R_{k1} + R_{k2} \\ R_{k1} - R_{k2} \end{bmatrix}, \begin{bmatrix} L_{dz} \\ L_{qz} \\ R_z \end{bmatrix}$$

$$= \begin{bmatrix} 0.5(L_{k1} + L_{k2}) + 2L_d \\ 0.5(L_{k1} + L_{k2}) + 2L_q \\ 0.5R_{sum} + 2R_s \end{bmatrix}.$$

III. Design and Stability Analysis of the SMCC

In this section, a sliding mode current controller (SMCC) is designed to improve the dynamic following performance of the stator current control. The key parameters of the SMCC should be designed quantitatively so that multiple adjustments are not required in engineering implementation.

A. Design of SMCC

To achieve fast and accurate tracking of the reference current, the tracking errors of the *dq*-axis stator currents are defined as the SMCC state variables:

$$\begin{bmatrix} x_d \\ x_q \end{bmatrix} = \begin{bmatrix} i^*_{dsum} - i_{dsum} \\ i^*_{qsum} - i_{qsum} \end{bmatrix} \tag{4}$$

where $i*$ *dsum* and $i*$ *qsum* are the *dq*-axis reference stator currents; x_d and x_q are the state variables of the SMCC, that is, the *dq*-axis tracking errors of the stator currents.

The integral sliding surface is selected as (5) to eliminate the static error and reduce the influence of high-frequency noise caused by the differential

$$\begin{bmatrix} s_d \\ s_q \end{bmatrix} = \begin{bmatrix} x_d + c_d \displaystyle\int_{-\infty}^{t} x_d dt \\ x_q + c_q \displaystyle\int_{-\infty}^{t} x_q dt \end{bmatrix}. \tag{5}$$

The differential of (5) is as follows:

$$\begin{bmatrix} \dot{s}_d \\ \dot{s}_q \end{bmatrix} = \begin{bmatrix} \dot{x}_d + c_d x_d \\ \dot{x}_q + c_q x_q \end{bmatrix} \tag{6}$$

where s_d and s_q are the *dq*-axis sliding surface functions, and when x_d and x_q converge to 0, the state variables are on the sliding surface; c_d and c_q are the integral coefficients.

The sliding mode motion goes through two stages in turn: reaching and stabilizing at the sliding mode surface. To improve the dynamic performance of the reaching process, the exponential reaching law is introduced:

$$\begin{bmatrix} \dot{s}_d \\ \dot{s}_q \end{bmatrix} = -\begin{bmatrix} k_{id}\mathrm{sgn}(s_d) + k_{ed}s_d \\ k_{iq}\mathrm{sgn}(s_q) + k_{eq}s_q \end{bmatrix} \tag{7}$$

where

$$\mathrm{sgn}(s) = \begin{cases} 1 & s > 0 \\ 0 & s = 0 \\ -1 & s < 0 \end{cases}$$

(7) is composed of isokinetic and exponential reaching terms. k_{id} and k_{iq} are the isokinetic reaching coefficients, which are also called the switching gains; k_{ed} and k_{eq} are the exponential reaching coefficients; and sgn(s) is a sign function.

Combining (3), (4), (6), and (7), the SMCC control law without considering disturbances is obtained as follows:

$$\begin{aligned} \begin{bmatrix} u_{dsum} \\ u_{qsum} \end{bmatrix} = & \begin{bmatrix} L_{dz0} & 0 \\ 0 & L_{qz0} \end{bmatrix} \begin{bmatrix} k_{id}\mathrm{sgn}(s_d) + k_{ed}s_d + c_d x_d \\ k_{iq}\mathrm{sgn}(s_q) + k_{eq}s_q + c_q x_q \end{bmatrix} \\ & + \begin{bmatrix} R_{z0} & \omega L_{qz0} \\ -\omega L_{dz0} & R_{z0} \end{bmatrix} \begin{bmatrix} i_{dusm} \\ i_{qsum} \end{bmatrix} + \begin{bmatrix} 0 \\ 2\omega\psi_{sm0} \end{bmatrix}. \end{aligned} \tag{8}$$

B. Traditional Stability Analysis

SMC is a nonlinear control method that can use the Lyapunov function to judge the stability. That is, if there is a positive definite and continuous function V related to the sliding mode surface function s, which satisfies the criterion (9), then the state variable will be stable on the sliding mode surface

$$1)\ \lim_{|s|\to\infty} V(s) = \infty,\ 2\ \dot{V}(s) < 0, s \neq 0. \tag{9}$$

Taking the q-axis sliding mode surface function as an example, the Lyapunov function can be defined as follows:

$$V_q = \frac{1}{2}s_q^2. \tag{10}$$

Combining (3), (4), (6), and (8), (10) is differentiated

$$\dot{V}_q = s_q\dot{s}_q = \left(-k_{iq}s_q\mathrm{sgn}(s_q) - k_{eq}s_q^2 - \frac{f_q s_q}{L_{qz0}}\right). \tag{11}$$

Scale (11) is as follows:

$$\dot{V}_q \le \left(-k_{iq}\left|s_q\right| + \left|\frac{f_q}{L_{qz0}}\right|\left|s_q\right|\right). \tag{12}$$

Combining (9), the stability range of k_{iq} is as follows:

$$k_{iq} \ge \left|\frac{f_q}{L_{qz0}}\right|. \tag{13}$$

Similarly, the stability range of k_{id} is obtained:

$$k_{id} \ge \left|\frac{f_d}{L_{dz0}}\right|. \tag{14}$$

However, the above method cannot determine the maximum time required for the state variable to reach the sliding surface. If the time is too long, it is meaningless in some situations such as the rapid change of the current caused by the stator changeover, and may even cause current divergence.

C. Improved Stability Criterion and Parameter Design

To make the state variables reach the sliding mode surface within the time of the stator changeover, an improved stability judgment method is proposed to quantitatively obtain an appropriate switching gain.

First, the Lyapunov stability criterion is modified

$$\dot{V} \le -\alpha V^{1/2}. \tag{15}$$

Transforming and integrating (15) leads to

$$\int_0^t \frac{\dot{V}}{V^{1/2}}dt = 2(V^{1/2}(t) - V^{1/2}(0)) \le -\alpha t. \tag{16}$$

Assuming that the initial state is known, the sliding mode state variable can reach the sliding mode surface within a finite time t_r, that is, $V(t_r)$ approaches zero. Then, the reaching time t_r can be rewritten as follows:

$$t_r \le \frac{2V_q^{1/2}(0)}{\alpha}. \tag{17}$$

During the stator changeover process of the train, the time required for the current attenuation or recovery process is approximately 0.25 s. In addition, the magnitude of the stator

current in DF mode does not exceed 1900 A. According to (4), (5), and (10), (17) is rewritten as follows:

$$\frac{2\sqrt{0.5(x_q(0)+c_q\int_{-\infty}^{t}x_q(0)dt)^2}}{\alpha}\geq\frac{\sqrt{2}x_q^2(0)}{\alpha}$$
$$=\frac{\sqrt{2}i^*_{qsum}}{\alpha}\geq t_r. \tag{18}$$

Assuming $i*$ *qsum* is 1900 A, α is selected as 10 748 to meet the required speed of reaching the sliding surface. That is, the following speed of stator current required for stator changeover is satisfied.

Then, combining (10), (11), and (15), the switching gain can be analyzed as follows:

$$\dot{V}_q=-k_{iq}s_q\mathrm{sgn}(s_q)-k_{eq}s_q^2-\frac{f_qs_q}{L_{qz0}}\leq-\alpha\frac{s_q}{\sqrt{2}}. \tag{19}$$

The discussion based on sgn(s_q) is as follows:

$$\begin{cases}k_{iq}\geq-\frac{\alpha}{\sqrt{2}}+k_{eq}s_q+\frac{f_q}{L_{qz0}}, & s_q<0\\ k_{iq}\geq\frac{\alpha}{\sqrt{2}}-k_{eq}s_q-\frac{f_q}{L_{qz0}}, & s_q>0.\end{cases} \tag{20}$$

Assuming that the disturbance is bounded, scaling (20) and combining (18), k_{iq} can be obtained as follows:

$$k_{iq}=\frac{i^*_{qsum}}{0.25}+\left|\frac{f_q}{L_{qz0}}\right|. \tag{21}$$

Similarly, to obtain the dynamic tracking performance of the *d*-axis current synchronized with the *q*-axis current, k_{id} is expressed as (22). Moreover, the values of k_{iq} and k_{id} will be held until the changeover process is completed

$$k_{id}=\frac{i^*_{qsum}}{0.25}+\left|\frac{f_d}{L_{dz0}}\right|. \tag{22}$$

According to the above analysis, the quantitative and real-time selection method of the SMCC switching gain is obtained. In addition, the effect of the exponential reaching term is ignored when analyzing the switching gain. To further improve the quality of the reaching sliding surface, the exponential reaching term is improved as follows:

$$\begin{bmatrix}\dot{s}_d\\ \dot{s}_q\end{bmatrix}=-\begin{bmatrix}k_{id}\mathrm{sgn}(s_d)+k_{ed}|s_d|^\gamma s_d\\ k_{iq}\mathrm{sgn}(s_q)+k_{eq}|s_q|^\gamma s_q\end{bmatrix}. \tag{23}$$

Among them, $0<\gamma<1$. By analyzing the exponential reaching term in (23), it can be seen that when the state variable does not reach the sliding mode surface and is far away from the surface, that is, $|s|>1$, the reaching speed of the state variable will be increased with the new reaching law. When the state variable is close to the surface, that is, $|s|<1$, the speed of reaching the surface will be appropriately slowed down. Therefore, the resulting chattering can be attenuated as the state variable crosses the sliding surface and the sign of *s* is changed.

The schematic diagram of the SMCC is shown in Fig. 3.

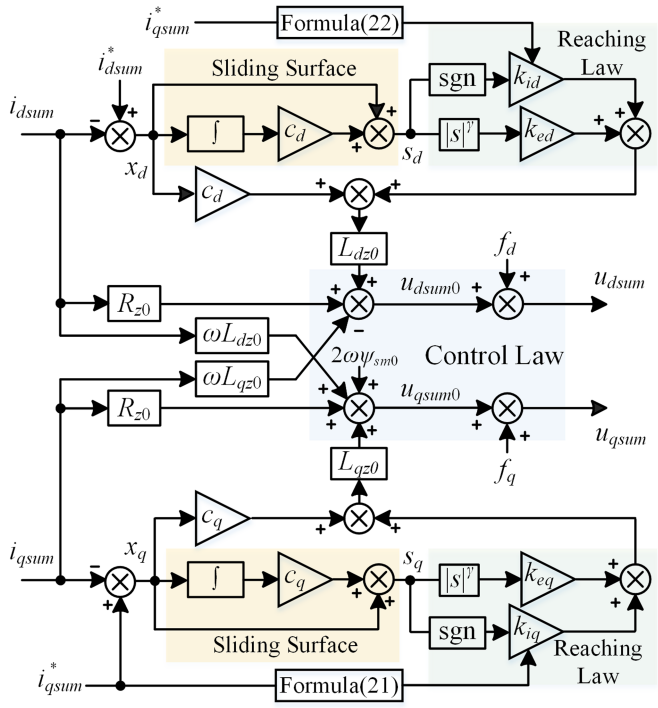

Fig. 3. Schematic diagram of the SMCC.

IV. Design and Stability Analysis of the SMDO

The existence of disturbances makes of the SMCC switching gain large enough to obtain the corresponding robustness, which will bring undesirable chattering. Therefore, to further improve the robustness and reduce the chattering, an SMDO is designed to estimate the disturbance and compensate for the SMCC.

A. Design of the SMDO

When designing the SMDO, the premise of accurately estimating the disturbance is that the observed current converges to the actual current. Therefore, to clarify the input and observation variables of the SMDO, Model (3) is rewritten as follows:

$$\begin{bmatrix}\frac{di_{dsum}}{dt}\\ \frac{di_{qsum}}{dt}\end{bmatrix}=\begin{bmatrix}-\frac{R_{z0}}{L_{dz0}} & \frac{\omega L_{qz0}}{L_{dz0}}\\ -\frac{\omega L_{dz0}}{L_{qz0}} & -\frac{R_{z0}}{L_{qz0}}\end{bmatrix}\begin{bmatrix}i_{dsum}\\ i_{qsum}\end{bmatrix}$$
$$+\begin{bmatrix}\frac{1}{L_{dz0}} & 0\\ 0 & \frac{1}{L_{qz0}}\end{bmatrix}\begin{bmatrix}u_{dsum}\\ u_{qsum}\end{bmatrix}$$
$$-\begin{bmatrix}0\\ \frac{2\omega\psi_{sm0}}{L_{qz0}}\end{bmatrix}-\begin{bmatrix}\frac{1}{L_{dz0}} & 0\\ 0 & \frac{1}{L_{qz0}}\end{bmatrix}\begin{bmatrix}f_d\\ f_q\end{bmatrix}. \tag{24}$$

The sliding surface function of the SMDO is defined as

$$\begin{bmatrix}e_{dsum}\\ e_{qsum}\end{bmatrix}=\begin{bmatrix}\hat{i}_{dsum}-i_{dsum}\\ \hat{i}_{qsum}-i_{qsum}\end{bmatrix} \tag{25}$$

where e_{dsum} and e_{qsum} are also the current observation errors.

The observation equation is as follows:

$$\begin{aligned}\begin{bmatrix}\frac{d\hat{i}_{dsum}}{dt}\\ \frac{d\hat{i}_{qsum}}{dt}\end{bmatrix} &= \begin{bmatrix}-\frac{R_{z0}}{L_{dz0}} & \frac{\omega L_{qz0}}{L_{dz0}}\\ -\frac{\omega L_{dz0}}{L_{qz0}} & -\frac{R_{z0}}{L_{qz0}}\end{bmatrix}\begin{bmatrix}\hat{i}_{dsum}\\ \hat{i}_{qsum}\end{bmatrix}\\ &+\begin{bmatrix}\frac{1}{L_{dz0}} & 0\\ 0 & \frac{1}{L_{qz0}}\end{bmatrix}\begin{bmatrix}u_{dsum}\\ u_{qsum}\end{bmatrix}\\ &-\begin{bmatrix}0\\ \frac{2\omega\psi_{sm0}}{L_{qz0}}\end{bmatrix}-\begin{bmatrix}U_{dsmo}\\ U_{qsmo}\end{bmatrix}\end{aligned} \tag{26}$$

where

$$\begin{bmatrix}U_{dsmo}\\ U_{qsmo}\end{bmatrix} = \begin{bmatrix}g_d\mathrm{sgn}(e_{dsum})\\ g_q\mathrm{sgn}(e_{qsum})\end{bmatrix}$$

$\hat{i}_{dsum}$ and $\hat{i}_{qsum}$ are the estimated values of i_{dsum} and i_{qsum}, respectively; U_{dsmo} and U_{qsmo} are the sliding mode functions of the SMDO, which contain the estimated values of the disturbances; and g_d and g_q are the sliding mode gains of the SMDO.

From (24) and (26), the error equation can be obtained as follows:

$$\begin{aligned}\begin{bmatrix}\frac{de_{dsum}}{dt}\\ \frac{de_{qsum}}{dt}\end{bmatrix} &= \begin{bmatrix}-\frac{R_{z0}}{L_{dz0}} & \frac{\omega L_{qz0}}{L_{dz0}}\\ -\frac{\omega L_{dz0}}{L_{qz0}} & -\frac{R_{z0}}{L_{qz0}}\end{bmatrix}\begin{bmatrix}e_{dsum}\\ e_{qsum}\end{bmatrix}\\ &+\begin{bmatrix}\frac{f_d}{L_{dz0}}-g_d\mathrm{sgn}(e_{dsum})\\ \frac{f_q}{L_{qz0}}-g_q\mathrm{sgn}(e_{qsum})\end{bmatrix}.\end{aligned} \tag{27}$$

Decoupling the dq-axis error equation allows the errors to converge without interference from the coupling terms. The new observation equation and error equation are obtained as (28) and (29), respectively.

$$\begin{aligned}\begin{bmatrix}\frac{d\hat{i}_{dsum}}{dt}\\ \frac{d\hat{i}_{qsum}}{dt}\end{bmatrix} &= \begin{bmatrix}-\frac{R_{z0}}{L_{dz0}} & \frac{\omega L_{qz0}}{L_{dz0}}\\ -\frac{\omega L_{dz0}}{L_{qz0}} & -\frac{R_{z0}}{L_{qz0}}\end{bmatrix}\begin{bmatrix}\hat{i}_{dsum}\\ \hat{i}_{qsum}\end{bmatrix}\\ &+\begin{bmatrix}\frac{1}{L_{dz0}} & 0\\ 0 & \frac{1}{L_{qz0}}\end{bmatrix}\begin{bmatrix}u_{dsum}\\ u_{qsum}\end{bmatrix}\\ &-\begin{bmatrix}0\\ \frac{2\omega\psi_{sm0}}{L_{qz0}}\end{bmatrix}-\begin{bmatrix}U_{dsmo}\\ U_{qsmo}\end{bmatrix}\\ &+\begin{bmatrix}0 & -\frac{\omega L_{qz0}}{L_{dz0}}\\ \frac{\omega L_{dz0}}{L_{qz0}} & 0\end{bmatrix}\begin{bmatrix}e_{dsum}\\ e_{qsum}\end{bmatrix}\end{aligned} \tag{28}$$

$$\begin{aligned}\begin{bmatrix}\frac{de_{dsum}}{dt}\\ \frac{de_{qsum}}{dt}\end{bmatrix} &= \begin{bmatrix}-\frac{R_{z0}}{L_{dz0}} & 0\\ 0 & -\frac{R_{z0}}{L_{qz0}}\end{bmatrix}\begin{bmatrix}e_{dsum}\\ e_{qsum}\end{bmatrix}\\ &+\begin{bmatrix}\frac{f_d}{L_{dz0}}-g_d\mathrm{sgn}(e_{dsum})\\ \frac{f_q}{L_{qz0}}-g_q\mathrm{sgn}(e_{qsum})\end{bmatrix}.\end{aligned} \tag{29}$$

B. Stability Analysis of the SMDO

To verify the convergence of the observation errors, taking the d-axis error as an example, combining (29), the following inequality needs to be satisfied:

$$\begin{aligned}\dot{V}_{dsmo} &= e_{dsum}\dot{e}_{dsum}\\ &= \frac{-R_{z0}e_{dsum}^2+e_{dsum}f_d}{L_{dz0}}-g_de_{dsum}\mathrm{sgn}(e_{dsum})<0.\end{aligned} \tag{30}$$

The discussion is based on $\mathrm{sgn}(e_{dsum})$ as follows:

$$\begin{cases} g_d > \frac{-R_{z0}e_{dsum}+f_d}{L_{dz0}}, e_{dsum}>0\\ g_d > \frac{R_{z0}e_{dsum}-f_d}{L_{dz0}}, e_{dsum}<0.\end{cases} \tag{31}$$

It can be combined as follows:

$$g_d > \frac{-R_{z0}\left|e_{dsum}\right|+\mathrm{sgn}(e_{dsum})f_d}{L_{dz0}}. \tag{32}$$

In practice, the switching gain of the SMDO should be as small as possible within the range of (32) to avoid excessive observation error and chattering.

Similarly, the range of g_q can be obtained as follows:

$$g_q > \frac{-R_{z0}\left|e_{qsum}\right|+\mathrm{sgn}(e_{qsum})f_q}{L_{qz0}}. \tag{33}$$

The schematic diagram of the SMDO is shown in Fig. 4.

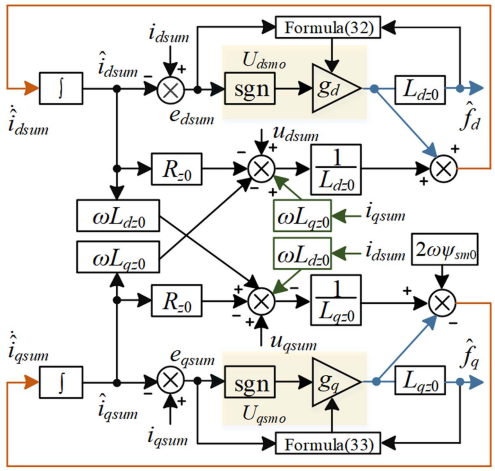

Fig. 4. Schematic diagram of the SMDO.

After the estimated disturbance is used as the compensation, (21) and (22) are rewritten as follows:

$$k_{iq} = \frac{i_{qsum}^*}{0.25}+\left|\frac{f_q-U_{qsmo}}{L_{qz0}}\right| \tag{34}$$

$$k_{id} = \frac{i_{qsum}^*}{0.25}+\left|\frac{f_d-U_{dsmo}}{L_{dz0}}\right|. \tag{35}$$

Since the disturbance is compensated by the SMDO, the switching gain of the SMCC does not need to be larger to enhance robustness thus further reducing the current chattering.

In summary, the closed-loop control diagram of the LSLSM based on the SMCC combined with the SMDO is shown in Fig. 5.

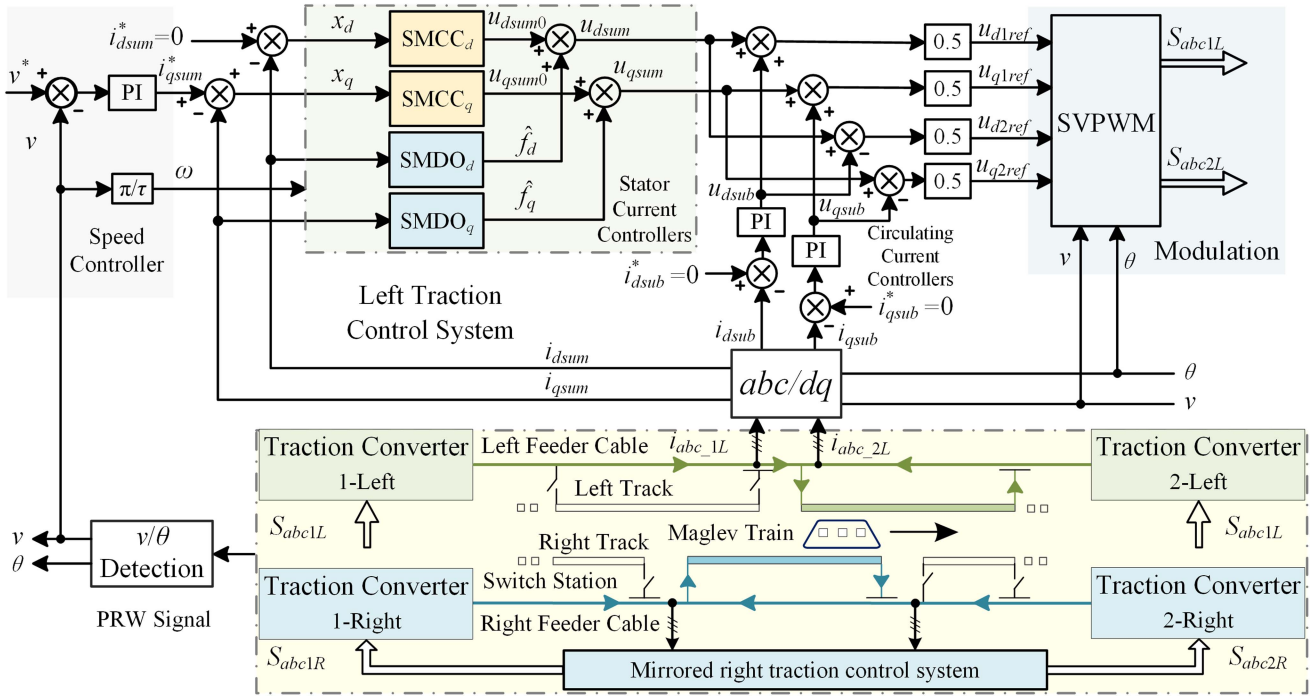

Fig. 5. Closed-loop control diagram of the LSLSM based on the SMCC combined with the SMDO.

V. Experimental Results

A. HIL Experimental Platform

To verify the control performance of the high-speed maglev train traction system in the laboratory, an HIL experimental platform for high-speed maglev transportation system is built, as shown in Fig. 6. The HIL experimental platform is mainly composed of a traction control system, an HIL test system, and a signal conditioning unit, as shown in Fig. 6(a). The physical platform is shown in Fig. 6(b).

The traction control system includes a motor control unit (MCU) and four converter control units (CCUs). The MCU mainly controls the speed and currents of the LSLSM, processes position signals, and interacts with other subsystems. The CCUs mainly accept the control instructions from the MCU and then output the corresponding voltage vectors by controlling the converter modules.

Four RT-LAB FPGA emulators are used as four sets of traction converter test subsystems, and two of the emulators are used as two sets of LSLSM test subsystems simultaneously. The above two subsystems together constitute the HIL test system. Finally, the host computer is connected with the Dolphin chassis of RT-LAB to realize the functions of model development and configuration, data acquisition, condition monitoring, and so on.

An active neutral point clamped (ANPC) three-level traction converter with a back-to-back structure provides variable frequency three-phase voltages for high-speed maglev train. The converter adopts a common dc bus structure with dual rectifiers and inverters, as shown in Fig. 7. In SF mode, the converter adopts direct mode (DM), that is, two sets of inverters are output in parallel to generate sufficient feed current when the train starts. In DF mode, transformer mode (TM) is adopted, that is, inverters are connected in series through a step-up transformer to overcome the back electromotive force when the train runs at high speed. The key parameters of the converter in DF mode are shown in Table I. The parameters of the LSLSM are shown in Table II.

TABLE I
Parameters of the Converter in DF Mode

Parameters	Value
Capacity (MVA)	24
Bus voltage (V)	5000
Maximum amplitude of output line current (A)	950
Maximum amplitude of output phase voltage (V)	16132
Ratio of the output transformer	2.6

TABLE II
Parameters of the LSLSM

Experimental Parameters	Value
Stator resistance R_s (mΩ)	436.176
Motor d-axis inductance L_d (mH)	3.9153
Motor q-axis inductance L_q (mH)	3.4653
Mutual inductance M_{sm} (mH)	165
Stator pole pitch τ (m)	0.258
Gross weight of train M (t)	306.9
Control frequency f_s (kHz)	7.2
Stator segment length l_s (m)	1200
Feeder cable resistance R_k (mΩ/km)	58.33
Feeder cable inductance L_k (mH/km)	0.0713

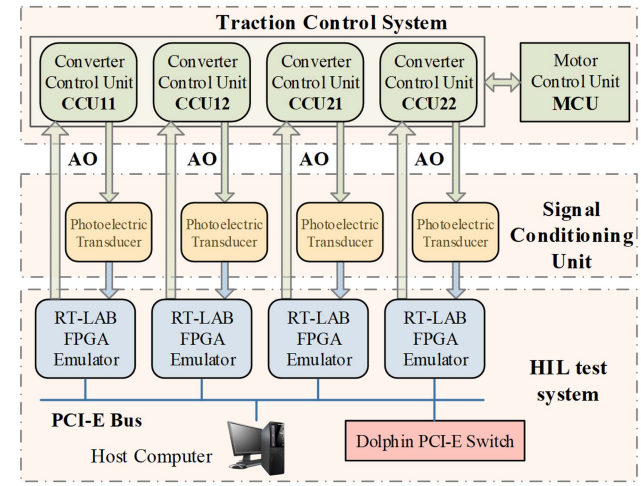

Fig. 6. Structure and platform of the high-speed maglev HIL experimental system. (a) Structure. (b) Platform.

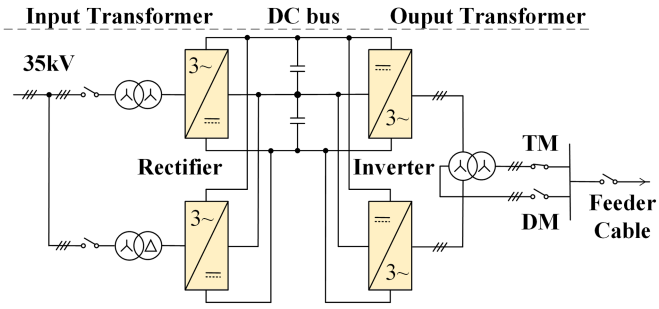

Fig. 7. Traction converter structure of high-speed maglev train in DF mode.

B. *Experimental Results of* dq*-Axis Stator Currents*

The LSLSM on the left side of the track serves as the research object. According to the operating target of the high-speed maglev train, the maximum target speed in the experiments is 600 km/h, and the target mileage is 56 km, which is also the total distance of the feed cable. The speed and mileage curves in the experiments are shown in Fig. 8.

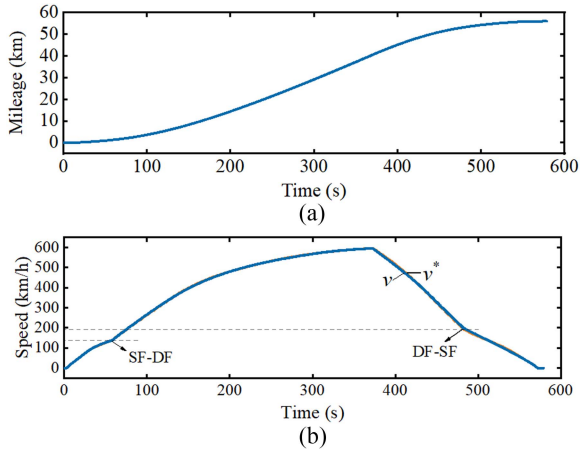

Fig. 8. Experimental results of the speed and mileage. (a) Speed. (b) Mileage.

TABLE III
CONTROLLER PARAMETERS

Controller	Parameters	value
PI	k_p	10
	k_i	20
SMCC	c	20
	k_{id}	Formula(35)
	k_{iq}	Formula(34)
	k_{ed}	100
	k_{eq}	100
SMDO	g_d	Formula(32)
	g_q	Formula(33)

In the experiments, the stator current loop in DF mode adopts three control strategies of PI-VFDC, SMCC, and SMCC combined with SMDO, denoted as Strategy I, II, and III, respectively. The main stator current controller parameters of the three strategies are shown in Table III.

Since the disturbance caused by inductance perturbation is more obvious at high speed, the total inductance parameter composed of the motor inductance and the feeder cable inductance jumps to 1.5 times the initial value at the mileage of 7.57 km, and recovers at 7.95 km, so as to verify the robustness of the control strategies. The total inductance L_z is expressed as

$$L_z = L_{k1} + L_{k2} + L_d + L_q. \tag{36}$$

The *dq*-axis stator currents of Strategy I are shown in Fig. 9. Fig. 9(a) shows that due to the *dq*-axis current coupling effect in DF mode, i_{dsum} produces large transient fluctuations when i_{qsum} varies rapidly during the changeover process, and this is more obvious at high speed. When the inductance parameter is perturbed, the fluctuations are particularly obvious. Fig. 9(b) shows that taking the stator changeover position at 14.94 km as an example, the fluctuation of i_{dsum} reaches 121.5 A. At the same time, i_{qsum} has an obvious tracking lag less than 0.1 s during the stator changeover process. In Fig. 9(c), at the moment of inductance parameter perturbation, the fluctuations of i_{dsum} and i_{qsum} reach 460 A and 260 A, respectively. In the process of

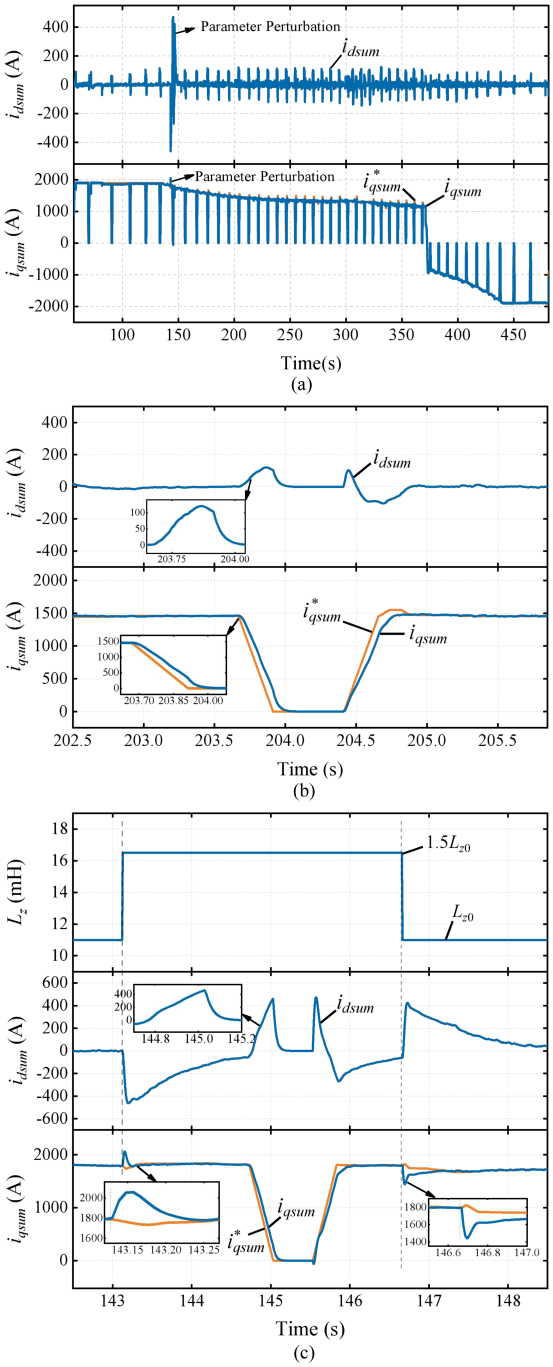

Fig. 9. Experimental results of Strategy I. (a) *dq*-axis currents in DF mode. (b) *dq*-axis currents during the changeover process without parameter perturbation. (c) *dq*-axis currents with inductance perturbation.

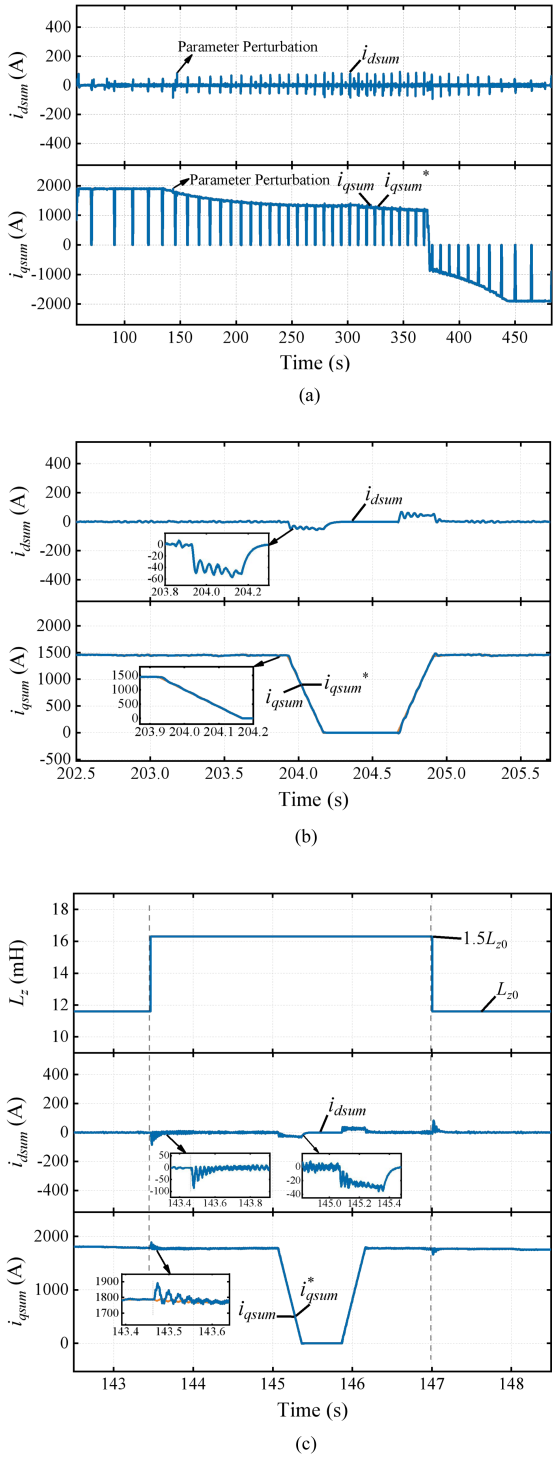

Fig. 10. Experimental results of Strategy II. (a) *dq*-axis currents in DF mode. (b) *dq*-axis currents during the changeover process without parameter perturbation. (c) *dq*-axis currents with inductance perturbation.

parameter perturbation, the fluctuation of i_{dsum} reaches 470 A during the changeover process. The above current fluctuations all require a long recovery time. The experimental results indicate that the dynamic tracking performance and robustness of the traditional PI-VFDC current control strategy are insufficient.

The *dq*-axis currents of strategy II are shown in Fig. 10. Fig. 10(a) shows that the fluctuations of i_{dsum} at each changeover position are suppressed by approximately half. Fig. 10(b) shows that at the same changeover position as in Fig. 9(b), the fluctuation of i_{dusm} reaches 57.9 A. Importantly, i_{qusm} has almost no delay in tracking the reference current during the changeover process. In Fig. 10(c), at the moment of inductance perturbation, the current fluctuations of i_{dsum} and i_{qsum} reach 86.5 A and

TABLE IV
COMPARISON OF EXPERIMENTAL RESULTS

Experiment Conditions		Results Comparison		
		I	II	III
Changeover position at 14.94 km	Δi_{dsum} (A)	121.5	57.9	24.7
	delay of i_{qsum} (s)	0.1	<0.01	<0.01
Moment of L_z perturbation	Δi_{dsum} (A)	460	86.5	22.8
	Δi_{qsum} (A)	260	102	27.1
Changeover in L_z perturbation	Δi_{dsum} (A)	470	36.1	18.8

102 A, respectively. In the process of parameter perturbation, the current fluctuation of i_{dsum} reaches 36.1 A during the changeover process. According to the design of the SMCC and the selection of switching gain, the dynamic tracking performance of the current loop of Strategy II is greatly improved compared with Strategy I. Furthermore, the recovery time of the current fluctuations is shortened. However, the robustness of the current loop still needs to be further improved, and there is current chattering during the recovery of current fluctuations.

The *dq*-axis currents of strategy III are shown in Fig. 11. Fig. 11(a) shows that the fluctuations of i_{dsum} at each changeover position are further suppressed by using the SMDO to compensate the disturbances. Fig. 11(b) shows that at the same changeover position as in Fig. 9(b), the fluctuation of i_{dusm} only reaches 24.7 A, and the tracking performance of i_{qsum} still maintains almost no delay effect during the changeover process. In Fig. 11(c), at the moment of inductance perturbation, the current fluctuations of i_{dsum} and i_{qsum} only reach 22.8 A and 27.1 A, respectively. In the process of parameter perturbation, the current fluctuation of i_{dsum} only reaches 18.8 A during the changeover process. Compared with Strategy II, the current fluctuations caused by the stator changeover and parameter perturbation are further suppressed, and the chattering in the recovery process of current fluctuations is also significantly suppressed. Strategy III greatly improves the control performance of the stator current under complex operating conditions.

The important results of the three control strategies are compared in Table IV.

To further verify the effectiveness of the proposed method to obtain the quantitative SMCC switching gain suitable for the changeover process, further experiments are carried out as follows. Since the current changes only 0.25 s during the changeover process, the current change rate is the largest when i_{qsum} is the maximum limit value of 1900 A. To meet the requirement of the current following speed, according to (34), k_{iq} should be selected as 7600. The stator current control adopts Strategy III. At the same changeover position of 6.42 km, the values of k_{iq} are taken as 4000, 7600, and 12000 for three sets of experiments, and the remaining parameters of Strategy III remain unchanged. The experimental results are shown in Fig. 12. The results shows that k_{iq} of 4000 and 12000 cause obvious deficiencies of current following speed and current chattering, respectively. Therefore, the proposed method to obtain the SMCC switching gain reconciles the contradiction between the current chattering and insufficient following speed.

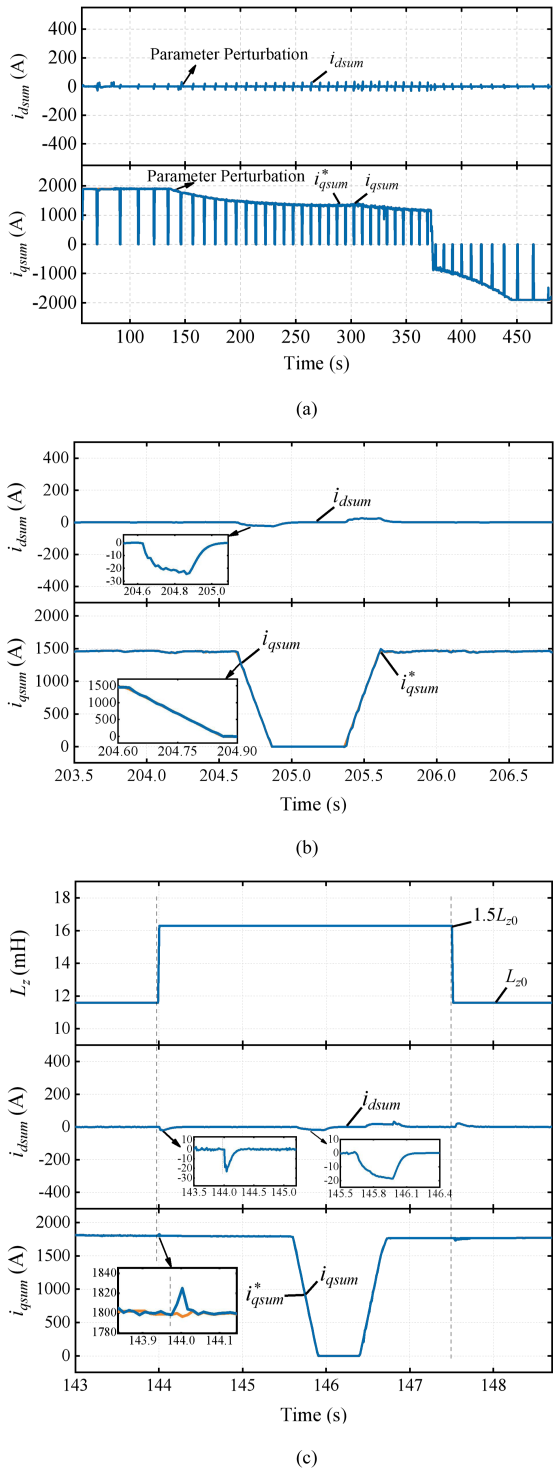

Fig. 11. Experimental results of Strategy III. (a) *dq*-axis currents in DF mode. (b) *dq*-axis currents during the changeover process without parameter perturbation. (c) *dq*-axis currents with inductance perturbation.

In summary, the traditional current control strategy of the LSLSM in DF mode has the shortcomings of poor current following performance, large current fluctuations, and slow recovery speed of the current fluctuations. The current control strategy based on the SMCC has satisfactory dynamic tracking

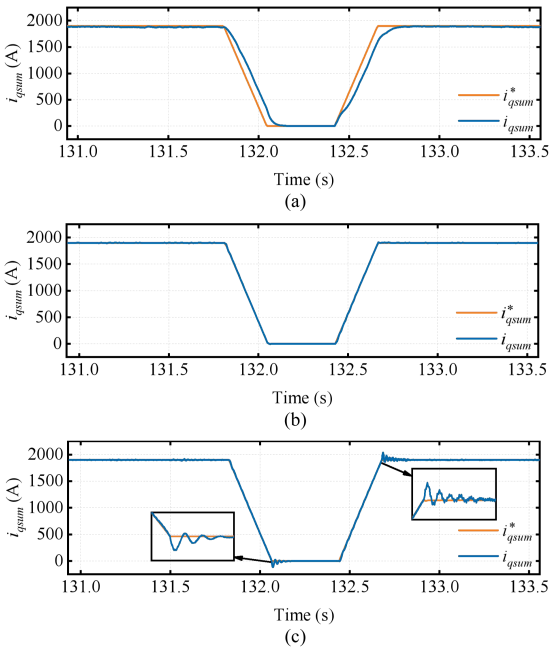

Fig. 12. Experimental results of current follow performance during the changeover process with Strategy III. (a) $k_{iq} = 4000$. (b) $k_{iq} = 7600$. (c) $k_{iq} = 12\,000$.

performance. The strategy based on the SMCC and SMDO further improves the robustness and suppresses the chattering.

VI. Conclusion

The mathematical model of the LSLSM used in high-speed maglev train in DF mode has been optimized. The SMCC and SMDO are designed based on this model. To meet the current following speed required for the stator changeover, a method to quantitatively obtain a suitable SMCC switching gain is proposed by improving the Lyapunov stability criterion. Then, the SMDO is designed to compensate the disturbance, thereby improving the robustness of the stator current control and suppressing the chattering. As verified by experimental results, the proposed strategy provides satisfactory robustness and dynamic tracking performance.

The proposed strategy not only reduces the complexity of the algorithm but also pays more attention to quantitatively obtaining the key parameters of the controller to avoid multiple debugging. This strategy is also applicable to other large inertia or high-power motion systems.

References

[1] Y. Zhang, G. Qing, Z. Zhang, J. Li, and H. Chen, "Calculation and simulation of propulsion power supply system for high-speed maglev train," in *Proc. IEEE Veh. Power Propulsion Conf.*, 2020, pp. 1–5.

[2] Hyung-Woo Lee, Ki-Chan Kim, and Ju Lee, "Review of maglev train technologies," *IEEE Trans. Magn.*, vol. 42, no. 7, pp. 1917–1925, Jul. 2006.

[3] Y. Sun, J. Xu, C. Chen, and W. Hu, "Reinforcement learning-based optimal tracking control for levitation system of maglev vehicle with input time delay," *IEEE Trans. Instrum. Meas.*, vol. 71, 2022, Art. no. 7500813.

[4] Y. Sun, J. Xu, G. Lin, W. Ji, and L. Wang, "RBF neural network-based supervisor control for maglev vehicles on an elastic track with network time delay," *IEEE Trans. Ind. Inform.*, vol. 18, no. 1, pp. 509–519, Jan. 2022.

[5] J. Zhu, Q. Ge, and P. Sun, "Extended state observer-based sensorless control for high-speed maglev application in single feeding mode and double feeding mode," *IEEE Trans. Transp. Electrific.*, vol. 8, no. 1, pp. 1350–1361, Mar. 2022.

[6] U. Henning, R. Hoffmann, and J. Hochleitner, "Advanced converter and control components for TRANSRAPID," in *Proc. 17th Int. Conf. Magnetically Levitated Syst. Linear Drives*, 2002.

[7] G. Lv, Z. Zhang, Y. Liu, and T. Zhou, "Characteristics analysis of linear synchronous motor integrated with propulsion, levitation, and guidance in high-speed Maglev system," *IEEE Trans. Transp. Electrific.*, vol. 7, no. 4, pp. 3185–3193, Dec. 2021.

[8] P. Sun, Q. Ge, M. Zhao, J. Zhu, and B. Zhang, "Research on parameters identification strategy of high-speed maglev train in double-end power supply mode," in *Proc. 13th Int. Symp. Linear Drives Ind. Appl.*, 2021, pp. 1–5.

[9] J. Gao, C. Gong, W. Li, and J. Liu, "Novel compensation strategy for calculation delay of finite control set model predictive current control in PMSM," *IEEE Trans. Ind. Electron.*, vol. 67, no. 7, pp. 5816–5819, Jul. 2020.

[10] Z. Zhang, Z. Wang, X. Wei, Z. Liang, R. Kennel, and J. Rodriguez, "Space-vector-optimized predictive control for dual three-phase PMSM with quick current response," *IEEE Trans. Power Electron.*, vol. 37, no. 4, pp. 4453–4462, Apr. 2022.

[11] W. Tu, G. Luo, Z. Chen, C. Liu, and L. Cui, "FPGA implementation of predictive cascaded speed and current control of PMSM drives with two-time-scale optimization," *IEEE Trans. Ind. Inform.*, vol. 15, no. 9, pp. 5276–5288, Sep. 2019.

[12] X. Li, Z. Xue, X. Yan, L. Zhang, W. Ma, and W. Hua, "Low-complexity multivector-based model predictive torque control for PMSM with voltage preselection," *IEEE Trans. Power Electron.*, vol. 36, no. 10, pp. 11726–11738, Oct. 2021.

[13] M.-Y. Wang, Y.-J. Niu, R. Yang, Q. Tan, J.-L. Jiang, and L.-Y. Li, "A robust double closed-loop control scheme for PMLSM drives," *IEEE Access*, vol. 6, pp. 62645–62654, 2018.

[14] M. Kadjoudj, M. E. H. Benbouzid, C. Ghennai, and D. Diallo, "A robust hybrid current control for permanent-magnet synchronous motor drive," *IEEE Trans. Energy Convers.*, vol. 19, no. 1, pp. 109–115, Mar. 2004.

[15] Y. A. R. I. Mohamed and E. F. El-Saadany, "A current control scheme with an adaptive internal model for torque ripple minimization and robust current regulation in PMSM drive systems," *IEEE Trans. Energy Convers.*, vol. 23, no. 1, pp. 92–100, Mar. 2008.

[16] R. Zhang, Z. Yin, N. Du, J. Liu, and X. Tong, "Robust adaptive current control of a 1.2-MW direct-drive PMSM for traction drives based on internal model control with disturbance observer," *IEEE Trans. Transp. Electrific.*, vol. 7, no. 3, pp. 1466–1481, Sep. 2021.

[17] Y. A. R. I. Mohamed, "Design and implementation of a robust current-control scheme for a PMSM vector drive with a simple adaptive disturbance observer," *IEEE Trans. Ind. Electron.*, vol. 54, no. 4, pp. 1981–1988, Aug. 2007.

[18] F.-J. Lin, S.-G. Chen, M.-S. Huang, C.-H. Liang, and C.-H. Liao, "Adaptive complementary sliding mode control for synchronous reluctance motor with direct-axis current control," *IEEE Trans. Ind. Electron.*, vol. 69, no. 1, pp. 141–150, Jan. 2022.

[19] X. Li, C. Liu, S. Wu, S. Chi, and P. C. Loh, "Sliding-mode flux-weakening control with only single current regulator for permanent magnet synchronous motor," *IEEE Access*, vol. 7, pp. 131616–131626, 2019.

[20] Y. Xu, S. Li, and J. Zou, "Integral sliding mode control based deadbeat predictive current control for PMSM drives with disturbance rejection," *IEEE Trans. Power Electron.*, vol. 37, no. 3, pp. 2845–2856, Mar. 2022.

[21] Y. Jiang, W. Xu, C. Mu, and Y. Liu, "Improved deadbeat predictive current control combined sliding mode strategy for PMSM drive system," *IEEE Trans. Veh. Technol.*, vol. 67, no. 1, pp. 251–263, Jan. 2018.

[22] V. Repecho, D. Biel, and A. Arias, "Fixed switching period discrete-time sliding mode current control of a PMSM," *IEEE Trans. Ind. Electron.*, vol. 65, no. 3, pp. 2039–2048, Mar. 2018.

[23] Y. Wang, Y. Feng, X. Zhang, and J. Liang, "A new reaching law for antidisturbance sliding-mode control of PMSM speed regulation system," *IEEE Trans. Power Electron.*, vol. 35, no. 4, pp. 4117–4126, Apr. 2020.

[24] W. Xu, Y. Jiang, and C. Mu, "Novel composite sliding mode control for PMSM drive system based on disturbance observer," *IEEE Trans. Appl. Supercond.*, vol. 26, no. 7, Oct. 2016, Art. no. 0612905.

[25] J. Li, Y. Yang, C. Hua, and X. Guan, "Discrete-time sliding mode control based on disturbance observer applied to current control of permanent magnet synchronous motor," *IET Power Electron.*, vol. 14, no. 4, pp. 875–887, Jan. 2021.

[26] X. Zhang, B. Hou, and Y. Mei, "Deadbeat predictive current control of permanent-magnet synchronous motors with stator current and disturbance observer," *IEEE Trans. Power Electron.*, vol. 32, no. 5, pp. 3818–3834, May 2017.
[27] L. Qu, W. Qiao, and L. Qu, "Active-disturbance-rejection-based sliding-mode current control for permanent-magnet synchronous motors," *IEEE Trans. Power Electron.*, vol. 36, no. 1, pp. 751–760, Jan. 2021.
[28] P. Lin, Z. Wu, K.-Z. Liu, and X.-M. Sun, "A class of linear–nonlinear switching active disturbance rejection speed and current controllers for PMSM," *IEEE Trans. Power Electron.*, vol. 36, no. 12, pp. 14366–14382, Dec. 2021.
[29] Z. Hao et al., "Linear/nonlinear active disturbance rejection switching control for permanent magnet synchronous motors," *IEEE Trans. Power Electron.*, vol. 36, no. 8, pp. 9334–9347, Aug. 2021.
[30] X. Sun, J. Cao, G. Lei, Y. Guo, and J. Zhu, "A robust deadbeat predictive controller with delay compensation based on composite sliding-mode observer for PMSMs," *IEEE Trans. Power Electron.*, vol. 36, no. 9, pp. 10742–10752, Sep. 2021.
[31] Z. Gong, C. Zhang, X. Ba, and Y. Guo, "Improved deadbeat predictive current control of permanent magnet synchronous motor using a novel stator current and disturbance observer," *IEEE Access*, vol. 9, pp. 142815–142826, 2021.
[32] D. Ke, F. Wang, L. He, and Z. Li, "Predictive current control for PMSM systems using extended sliding mode observer with Hurwitz-based power reaching law," *IEEE Trans. Power Electron.*, vol. 36, no. 6, pp. 7223–7232, Jun. 2021.
[33] B. Wang, Z. Dong, Y. Yu, G. Wang, and D. Xu, "Static-errorless deadbeat predictive current control using second-order sliding-mode disturbance observer for induction machine drives," *IEEE Trans. Power Electron.*, vol. 33, no. 3, pp. 2395–2403, Mar. 2018.
[34] X. Sun, J. Cao, G. Lei, Y. Guo, and J. Zhu, "A composite sliding mode control for SPMSM drives based on a new hybrid reaching law with disturbance compensation," *IEEE Trans. Transp. Electrific.*, vol. 7, no. 3, pp. 1427–1436, Sep. 2021.
[35] X. Zhang, L. Sun, K. Zhao, and L. Sun, "Nonlinear speed control for PMSM system using sliding-mode control and disturbance compensation techniques," *IEEE Trans. Power Electron.*, vol. 28, no. 3, pp. 1358–1365, Mar. 2013.
[36] X. Zhang and Z. Li, "Sliding-mode observer-based mechanical parameter estimation for permanent magnet synchronous motor," *IEEE Trans. Power Electron.*, vol. 31, no. 8, pp. 5732–5745, Aug. 2016.

Xueqian Cao received the B.S. degree in electrical engineering from China University of Petroleum (East China), Qingdao, China, in 2018. He is currently working toward the Ph.D. degree in power electronics and power drives from the Institute of Electrical Engineering, Chinese Academy of Sciences, Beijing, China.

His research interests include high power converter, control of linear motors, and ac drives.

Qiongxuan Ge (Member, IEEE) received the B.S. degree from Nanchang University, Nanchang, China, in 1989, the M.S. and Ph.D. degrees from the University of Chinese Academy of Sciences, Beijing, China, in 1997 and 2007, respectively, all electrical engineering.

From 1989 to 1994, she was an Assistant Professor with the Electrical Engineering Department, Jiangxi University of Science and Technology, Ganzhou, China. From 1999 to 2006, she was an Associate Professor with the Institute of Electrical Engineering, Chinese Academy of Sciences, Beijing, China. Since 2007, she has been a Research Professor with the Research Centre of High Power Electronics and Linear Drive, Institute of Electrical Engineering, Chinese Academy of Sciences. Her research interests include high power converter and motor control.

Jinquan Zhu received the B.S. degree in automation from Hefei University of Technology, Hefei, China, in 2016, and the Ph.D. degree in power electronics and power drives from University of Chinese Academy of Sciences, Beijing, China, in 2021.

He joined the Institute of Electrical Engineering, Chinese Academy of Sciences, in 2022, where he is currently a Postdoctoral. His research interests include high power converter, control of linear motors and ac drives.

Ganlin Kong received the B.S. degree in automation from Tsinghua University, Beijing, China, in 2019. She is currently working toward the Ph.D. degree in power electronics and power drives with the Institute of Electrical Engineering, Chinese Academy of Sciences, Beijing, China.

Her research interests include high power converter, control of linear motors and ac drives.

Bo Zhang received the B.S. and M.S. degrees in electrical engineering from the Hebei University of Technology, Tianjin, China, in 2009 and 2012, respectively, and the Ph.D. degree in power electronics and power drives from University of Chinese Academy of Sciences, Beijing, China, in 2016.

In 2016, he joined the Institute of Electrical Engineering, Chinese Academy of Sciences, where he is currently an Associate Professor. His research interests include topology and control of high-power multilevel power converters, and high-speed maglev motor drive techniques.

Xiaoxin Wang received the B.S. and M.S. degrees in electrical engineering from the Harbin Institute of Technology, Harbin, China, in 2000 and 2002, respectively.

He joined the Institute of Electrical Engineering, Chinese Academy of Sciences, in 2002, where he is currently a Senior Engineer. His research interests include topology and control of high-power multilevel power converters, and high-speed maglev motor drive techniques.